**Article:**
Pan, X, Zhang, L and Huang, H (2022) Harmonic Cancellation by Adaptive Notch Filter based on Wavelet Package Transform for an MMCC-STATCOM. IEEE Transactions on Power Delivery, 37 (3). pp. 1834-1844. ISSN 0885-8977

https://doi.org/10.1109/TPWRD.2021.3099201

# Harmonic Cancellation by Adaptive Notch Filter based on Discrete Wavelet Packet Transform for an MMCC-STATCOM

Xuejiao Pan, Li Zhang, *Senior Member, IEEE,* Han Huang

***Abstract*—This paper presents an adaptive harmonic current extraction scheme using notch filters combined with a modified discrete wavelet-packet transform (DWPT). The scheme is applied to an MMCC-STATCOM for mitigating current harmonics distortion in a power line. The modified DWPT incorporates a data expansion technique to overcome the limitations of boundary effect. It identifies the rms values of the dominant harmonic elements of the non-stationary current in real-time, these being used to update the order and stop-frequency of a notch filter chain. This adaptive notch filter is embedded in the current control system for the MMCC-STATCOM to generate reference current. The results have shown that the modified DWPT tracks harmonic changes faster and more accurately than the conventional method. The technique enables the STATCOM to adapt quickly to load current changes, hence giving accurate elimination of current harmonics in real-time.**

***Index Terms*—Discrete Wavelet-Packet Transform (DWPT), Adaptive Notch Filter (ANF), multilevel modular cascaded converter-based STATCOM (MMCC-STATCOM).**

## I. Introduction

THE growing use of power electronic controlled-equipment, such as uncontrolled rectifiers, grid-tied converters for renewable sourced generators [1], and large traction drives [2], results in significant levels of harmonic current components drawn at the Point of Common Coupling (PCC). Consequently they cause PCC voltage distortion owing to the flow of harmonic current through the finite line impedance. Voltage and current harmonics degrade the quality of power supplied to customers, the power system operating stability, and the efficiency.

Research in harmonic current cancellation has resulted in various techniques aiming to separate the harmonic components from the fundamental current. One important device is the Static Compensator (STATCOM) [3]–[5] which is a flexible and effective tool for harmonic mitigation and for compensating reactive power. It uses a Voltage Source Inverter connected in parallel with the power line via a coupling impedance or a transformer to inject appropriate compensating current to the system. The development of modular multilevel cascaded converters (MMCC) [6] in the last two decades facilitates the applications of the STATCOM to medium and high voltage networks [7], [8]. The modular structure of a MMCC-STATCOM, having either full H-bridge or flying-capacitor converters as sub-modules, offers advantages of flexibility in generating the compensating current with the required waveform at a low switching frequency. The device is efficient and fault tolerant, with a small footprint [9]–[12].

Key to enabling any STATCOM to eliminate harmonics is its ability to identify and extract the harmonic elements, often time varying, in the load current. Advanced signal processing techniques in both time and frequency domains have been employed. Most well-known, in the time domain, is the Instantaneous Reactive Power Theory proposed by Akagi in 1983 [13]. This relies on separating the instantaneous active, reactive and harmonic powers from the apparent power measured in real-time. Subsequently it is possible to derive all harmonic current elements from the harmonic power at every sample instant. However, this method relies on distortion-free grid reference voltages for extraction of harmonic currents and hence would not work well in the presence of supply voltage harmonics or imbalance. An alternative approach is based on Synchronous Reference Frame (SRF) theory [14]. This operates by transforming load currents into a d-q reference frame rotating at the fundamental frequency, so that harmonic components become AC terms that can be extracted. The method needs a phase-locking loop for three-phase current transformation. It also requires a low-pass filter which must be tuned properly with a sufficiently low cut-off frequency yet adequate speed of response to follow load current changes.

Among techniques for harmonic analysis, the very familiar fast Fourier Transform (FFT) [15], [16] provides magnitude-frequency information with advantages of high accuracy and lower computational burden than the Discrete Fourier Transform (DFT). It suffers from poor detection of the time locality when the signal varies abruptly, and hence is most suited to stationary power signal analysis. To better describe non-stationary signals, the Short-Time Fourier Transform (STFT) has been a useful tool, though it relies on properly selecting the size of a time window and the window function must be well-localized.

The Wavelet Transform (WT) provides a different approach which can process non-stationary signals in both time and frequency domains [17]–[20]. Unlike the FFT which expands the signal in terms of sine waves, the WT uses wavelets which are generated in the form of translations and dilation of mother wavelets. These are irregular in shape with special scaling properties and localized in time, making them ideal for representing transient distorted electrical signals with no stationary features. Various WT implementations have been derived, such as the continuous wavelet transform (CWT)

The authors are with the School of Electrical Engineering, University of Leeds, Leeds, UK (e-mail: ml16xp@leeds.ac.uk; L.Zhang@leeds.ac.uk;han.huang@ge.com).

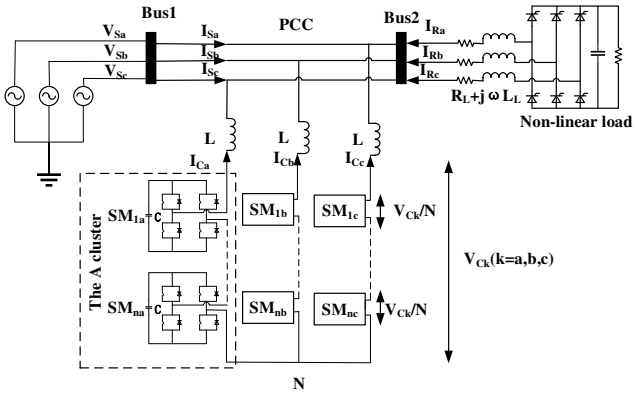


Fig. 1. Configuration of SSHB STATCOM.

[21] which has been shown to be computationally complex and hence not suitable for real-time use. The multi-resolution analysis [22], [23] and discrete wavelet transform (DWT) [24] reduce computation complexity and have been used in various power quality analysis work [25]–[27]. However these possess clear limitations since the signal is decomposed into approximations (low-frequency components) and details (high-frequency components), but only the former is processed. This leads to the loss of a certain information about the signal. The discrete wavelet packet transform (DWPT) can overcome this limitation. In this technique, a sampled signal series is decomposed into scaling and wavelet coefficients by convolution with both a high-pass and a low-pass filter at uniform frequency bands, and thus it can extract both high and low frequency elements of the signal.

In using DWPT and other WT techniques for processing sampled signals in real-time, certain issues require careful consideration particularly with time varying power signals. Proper selection of the mother wavelet, which must be based on the features of the signal analyzed, results in reduction of the computational burden and improved accuracy in the result. The boundary effects due to limited data samples will cause distortion of the reconstructed harmonic waveforms and hence inaccuracy of the detected harmonic components.

This paper proposes an adaptive harmonic current extraction scheme using notch filters combined with a modified discrete wavelet-packet transform (DWPT). The scheme is applied to control an MMCC-STATCOM which cancels the harmonic current on the power line. As is well known, the odd harmonics are generally dominant in power line current while even and inter-harmonics are negligibly small and this has been validated in [28], [29], hence the proposed scheme uses DWPT to identify only a selection of lower order odd harmonics. They are eliminated using a chain of notch filters [30], [31] with their rejection frequencies tuned to the identified values. To attenuate the residual even harmonics, arising from asymmetric load current, and small inter-harmonic elements on the power line current, the method adjusts the damping ratios of the notch filters to widen their stop frequency bands and this yields useful suppression of extra frequencies.

The modified DWPT employs the discrete Meyer as the mother wavelet, which is selected according to the criterion of minimum oscillation error. It also incorporates a data expansion technique to overcome the limitations of boundary effects due to insufficient data samples. The technique identifies the rms values of the dominant harmonic elements in the non-stationary current in accordance with the IEEE Standard 519-2014 [32] in real-time.

Section II of the paper outlines the configuration of the star-connected MMC-STATCOM. In Section III, the basic principle of the DWPT is reviewed and mother wavelet selection is discussed. The data expansion technique for DWPT is described in detail In Section IV. The complete adaptive harmonic current cancellation control scheme is discussed in Section V and validated in Section VI.

## II. Configuration of The MMCC-STATCOM

The configuration of the star-connected MMCC-STATCOM is shown in Fig.1. There is no link between the neutral points at the converter side and supply side. Each of the three phases consists of N serially connected H-bridge converter sub-modules, each having a floating capacitor maintaining its voltage at $V_{Ck}/N$, and hence generating (2N+1) voltage levels: 0, $\pm(1/N)V_{Ck}$, $\pm(2/N)V_{Ck}$ ..... $\pm V_{Ck}(k = a, b, c)$. The terminals of the three phase clusters are connected to the grid at the point of common coupling (PCC) through three single-phase filter reactors $L$. These reduce high frequency harmonics due to switching but naturally create time-delays for current flow. At the load side, a phase controlled rectifier with an $R-L$ load is applied. Not only can this emulate steady non-sinusoidal current flow, it can also imitate, by varying the phase angles, transient interruptions caused by sudden surge of load current or faults of switching operations.

The function of the STATCOM is to inject current to the grid at PCC point, which eliminates as much as possible the reactive/harmonic elements in the load current, and hence improve the quality of the grid supplied power. The PCC current is given as $I_{Sk} = I_{Ck} + I_{Rk}$.

## III. Principles of DWPT Technique

According to the principle of Wavelet Transform, any time series signal can be decomposed into a collection of small 'wavelets'. In the case of the DWPT, a sampled signal series is decomposed into the scaling and wavelet coefficients by convolution with both a high-pass and a low-pass filter.

### A. DWPT Principle Review

Assume a signal $P$, having $M$ samples, convolutes with a low-pass filter, $h_l$, and a high-pass filter, $g_l$ . These filters are quadrature mirror filters (QMFs) [33] and their relationship meets the following expression:

$$g(l) = (-1)^l h(L - l - 1) \tag{1}$$

where $l$ and $L$ are the order and length of the filter ($l = 0, 1, .....L - 1$) respectively. Since at every level of decomposition the signal is down sampled by a factor of 2, wavelet coefficients at any level $j$ for the $kth$ point in $2n$ and $2n + 1$ nodes are obtained by convolution with the filters $h$ and $g$ as follows

$$P_j^{2n}[k] = \sum_{l=0}^{L-1} h_l P_{j-1}^n[2k-l] \tag{2}$$

$$P_j^{2n+1}[k] = \sum_{l=0}^{L-1} g_l P_{j-1}^n[2k-l] \tag{3}$$

For $M$ samples of the original signal, the number $k$ of the wavelet coefficients in each node for the $jth$ layer satisfies the following equation:

$$k = M/2^j \tag{4}$$

So the wavelet coefficients in the nth node at the $jth$ layer are indicated by: $P_j^n[k] = 0, 1, 2....M/2^j$

Fig.2 shows the decomposition tree of the measured signal with a constant bandwidth up to level $j = 3$ , leading to the derivation of 8 nodes of the detail and approximation coefficients.

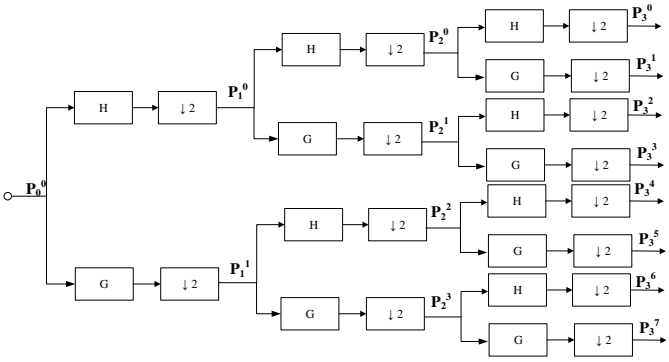


Fig. 2. DWPT data decomposition tree up to 3-levels.

Similar to the FFT technique, the original signal can be reconstructed or recovered through the characteristic coefficients obtained by the DWPT decomposition process, where the equation for reconstruction is given as:

$$P_{j-1}^n[2k-l] = \sum_{l=1}^{L} h_l^* P_j^{2n}[k] + \sum_{l=1}^{L} g_l^* P_j^{2n+1}[k] \tag{5}$$

Here $h_l^*$ and $g_l^*$ are the antithetic operators of the low-pass and high-pass filters $h_l$ and $g_l$ [34].

If a single odd harmonic is to be observed, the coefficients in other nodes in the same layer can be set to 0, and then through reconstructing process, the signal waveform of a specific frequency in the original signals can be obtained.

### B. Selection of Mother Wavelet

The choice of mother wavelet is crucial for accuracy and computational efficiency. High accuracy from a power signal depends on using the high order wavelet filters which can cope well with faster waveform response. Thus high-order mother wavelets are often chosen for harmonic element rms value calculations [35], [36]. However the computational complexity and the number of coefficients are correlated, hence these wavelet functions cause longer delays in signal analysis, making them more suitable for off-line stationary signal analysis, but not ideal for on-line tracking of non-stationary or transient variation signals.

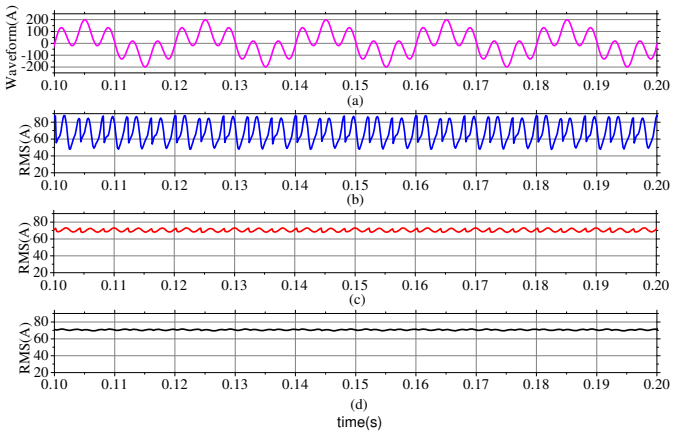


Fig. 3. (a) Original signal waveform. (a) RMS values of the 5th order element in the reconstructed signal by db8, (c) db30, (d) discrete meyer.

In this paper, three different wavelet functions are compared according to their performances in harmonic extraction accuracy and speed. These are Daubechies wavelet functions; db8 with 16 coefficients, db30 with 60 coefficients, and the discrete meyer with 98 coefficients. A synthetic waveform as shown in Fig. 3(a) is used for this study. It is composed of a fundamental and a 5th order harmonic with magnitude being 100 for both elements and is expressed as:

$$x(t) = 100sin(2\pi \times 50t) + 100sin(2\pi \times 250t) \tag{6}$$

Fig. 3(b) to (d) shows the rms value variations of the reconstructed $5th$ order harmonic using respectively the above said three wavelet functions. As can be seen, the reconstructed $5th$ order rms from the db8 wavelet presents the highest level fluctuations(30%), while waveform from using the db30 is more stable which is 4%. However it is the waveform from the discrete meyer which shows the minimum level of variations(1.5%). In quantifying this feature, a percentage oscillation error is defined as the maximum peak-peak rms value over the desired $100/\sqrt{2}$.

## IV. DWPT with Data Expansion

### A. Sample Frequency

Another important consideration for the DWPT application is the number of sampled data required for the maximum decomposition layer. This depends on the highest harmonic element in the original signal to be extracted. In the distorted load current, the odd harmonics such as the $3rd$, $5th$ up to $17th$ orders are the dominant elements. For effective extraction, the frequencies of these elements should be in the centers of their respective node, namely the frequency band. Also the signal should be decomposed continuously until the fundamental component is separated from all the other harmonic elements. Assuming the highest harmonic frequency in the signal is 3200 Hz, according to Nyquist criterion, the chosen sampling frequency should be twice of this value, i.e. 6400Hz. The decomposition layer $j$ is determined by the

maximum harmonic order to be extracted and the sampling frequency. In this case 5 decomposition levels are required in order to extract the fundamental and odd harmonics from $3rd$ to $63th$ order through coefficients $P_0^5$ to $P_{31}^5$ with a uniform frequency band of $100Hz$. All odd harmonics are in the central position within each band. The relationship is shown in table I [37], where it can be seen that the observable frequency range is evenly distributed among these nodes.

TABLE I
DECOMPOSED LAYERS ASSOCIATED WITH THE MAXIMUM HARMONIC ORDER AND SAMPLING FREQUENCY

| Maximum harmonic order | Sampling frequency $f_s(Hz)$ | Decomposed layers $j$ |
|---|---|---|
| $3rd$ | 400 | 1 |
| $7th$ | 800 | 2 |
| $15th$ | 1600 | 3 |
| $31st$ | 3200 | 4 |
| $63rd4$ | 6400 | 5 |

### B. Data Expansion for Real-time application

For on-line real-time tracking of harmonic components in the non-stationary signal, the signal decomposition is performed using the data collected continuously over a short time window. This is necessary especially for tracking transient surge currents due to faults or sudden load changes, hence to register the time of occurrences, and magnitudes and frequencies of any abnormalities. However for fast tracking, the time window per data processing may be narrow hence the number of data collected may be small, leading, consequently to insufficient data for performing multiple levels of data decomposition. For example, if a data window is set to 0.01 second, i.e. one half of a 50Hz period with sampling frequency of 6400 Hz, it yields 64 data samples. This data set is far too small to allow 5 level data decomposition, but further increasing the sampling rate adds more real-time computational cost and data noise. A simple approach to overcome this dilemma is to replicate the sampled data within each data window to the number required. Thus with data logged at each sample interval being x(m), it can be replicated as many times as needed. The resultant data number per sample interval can be stored into a two dimensional array as

$$y(m,i) = (-1)^i x(m) \tag{7}$$

where m represents number of samples per fixed time window which is 64 in this example, $i$ represents the number of replication per data window. In this way, the data in a sampling window, originally 64 samples, would be expanded to $64i$ in total. To ensure the number of data be sufficient for 5 level data decomposition and also the results are sufficiently accurate, results are compared for $i$ = 10, 50 and 100. Fig. 4 (a)-(d) shows, respectively, the variations of rms values of the reconstructed 5th order element obtained for using these three replication numbers and that without data expansion. Fig.4 (a) shows the highest level of rms variation without data expansion, the oscillation error (%), with the discrete meyer, is about 20%. With $i$ changing from 100 to 10, data samples from 6400, 3200 to 640 in Fig.4 (b) to (d), the corresponding error percentages are 1.5%, 5% and 8%, respectively. Thus, replicating to 6400 samples is chosen since it is the most accurate and the processing times for all cases are the same.

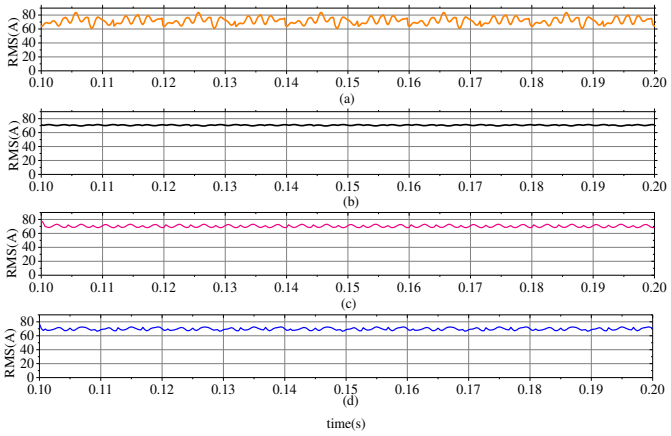


Fig. 4. Reconstructed 5th order element by discrete meyer (a) without data expansion, (b) with data expansion expanding to 6400 samples (c)3200 samples and (d)640 samples.

Note for the analysis without data expansion, the data window is extended to 2 fundamental periods, hence 256 samples in total are available, and consequently the data tracking speed is naturally slower.

### C. Boundary Distortion Reduction

The problem of edge effects in filtering would affect the accuracy of the DWPT results, due to that the convolution is performed on a signal with finite-length. Several conventional methods for correcting this effect have been developed [38]. In this work, the application of data expansion technique is shown effective in suppressing the edge distortion effect.

Implementation of the DWPT is performed from the beginning at every sample interval with the full set of data. Due to the data duplication, the edge distortion effect is significantly reduced. Fig. 5(b) shows the reconstructed $5th$ order harmonic waveform derived at two selected data points, one, 2874(black line), is at the middle of the data window and the other, 5998(red line), near the end. As can be seen both waveform conform well with the original one(blue line). There are little errors shown in amplitude, the small phase delay is due to data processing.

## V. DWPT-BASED ADAPTIVE HARMONIC CONTROL

In this study, the above DWPT algorithm is used for harmonic cancellation by the MMCC-STATCOM of Section II. The key element in the STATCOM filtering scheme is an adaptive multiple frequency band notch filter-chain, which consists of a number of single band-stop notch filters. The numbers of these filters and their parameters are updated according to the harmonics extracted by the DWPT operating online in real-time. Fig.6 illustrates the overall control strategy for the MMCC-STATCOM and comprises three main parts: the DWPT-based ANF, the cluster sub-module voltage balance

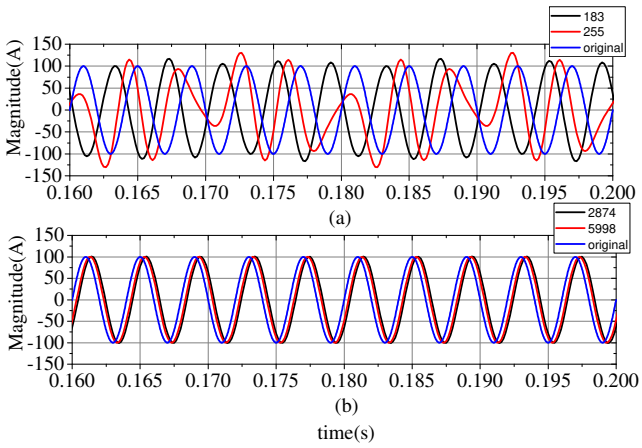


Fig. 5. Reconstructed signals by choosing different points (a) without and (b) with data expansion.

control, and overall current control block. The latter two parts are well-known and need not be described here.

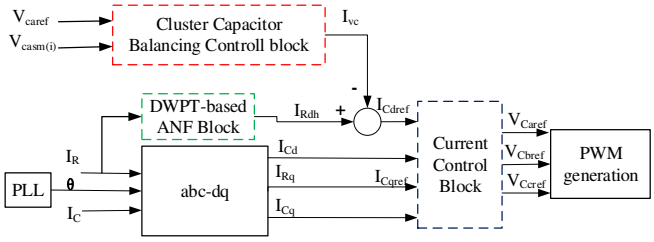


Fig. 6. Overall control strategy for the MMCC-STATCOM.

### A. DWPT-based ANF

A notch filter can effectively attenuate a harmonic element in the applied signal. The transfer function of a single notch filter is expressed as [39]:

$$T(s)_{NF} = \frac{s^2 + \omega_0^2}{s^2 + 2\sigma\omega_0 s + \omega_0^2} \tag{8}$$

where $\omega_0$ is the required stop frequency and $\sigma$ is the damping ratio which determines the width of the notch. To attenuate a range of even and inter-harmonic elements surrounding the dominant odd harmonics, the damping factor can be adjusted in order to widen the frequency stop-band. Fig.7 shows the Bode plot of a notch filter when the stop-frequency is set at the $5th$ order harmonic (1570 rad/s) with different damping ratios from 0.1 to 0.5. It is clear that dB values of harmonic elements close to the 5th order are substantially attenuated. However, larger damping ratio comes with a price of increased phase shift. A study using a system shown in Fig. 1 with load firing angle changing has been performed. The results are shown in Table II with $\sigma$ changing from 0.1 to 0.5 for periods 2, 3, 4 denoting firing angles 0°, 30°and 45° respectively. It is clear that the higher $\sigma$ yields lower THD of the resultant current waveform but a longer time delay in the current response. Especially when the damping ratio is around 0.5, the delay

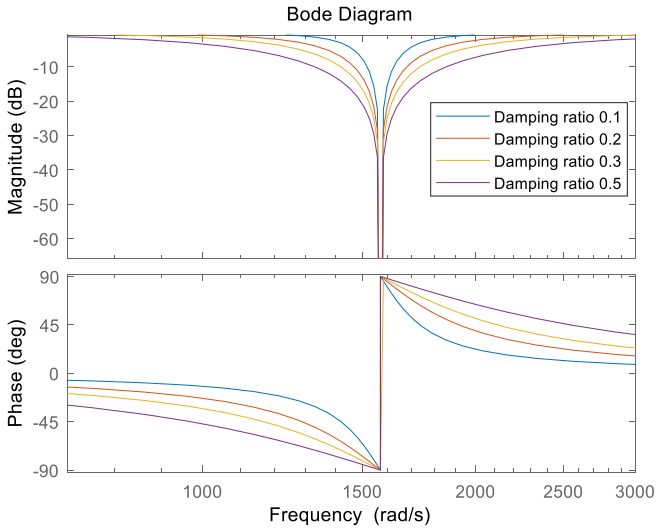


Fig. 7. Bode diagram for adaptive notch filters.

TABLE II
THD VALUES OF PCC CURRENT AND SETTLING TIME FOR DIFFERENT DAMPING RATIOS OF NOTCH FILTERS

| Damping ratio | Period 2 | Period 3 | Period 4 | Settling time(ms) |
|---|---|---|---|---|
| $\sigma$=0.1 | 2.04% | 2.77% | 4.77% | 11.445 |
| $\sigma$=0.2 | 1.91% | 2.74% | 4.44% | 14.634 |
| $\sigma$=0.3 | 1.85% | 2.56% | 4.1% | 17.236 |
| $\sigma$=0.5 | 1.75% | 2.34% | 3.7% | 21.103 |

time is about 21ms, twice as long as that when $\sigma$ is 0.1, so a compromise needs to be made. In this case, $\sigma$ = 0.2 is chosen.

The current harmonics in a power system may be time varying, correspondingly the frequencies of the chained notch filters need to be adjusted, hence being adaptive. The configuration of the adaptive notch filter with DWPT as harmonic element tracker is shown in Fig.8. As can be seen in this figure, $Re_1$ up to $Re_{17}$ are the reconstructed signals ranging from the fundamental to $17th$ harmonic, $j$ represents the number of notch filters required in the chain and $\omega(j)$ stores the selected harmonics to be eliminated. The selection is based on IEEE-519-2014 [32] standard, in which the allowed maximum harmonic current distortion is 4% from the $3rd$ to $11th$ harmonic and 2% between the $11th$ and $17th$. Thus when the ratio between the $13th$ or $17th$ harmonic and the fundamental is higher than 2%, this order is included in the notch frequencies $\omega(j)$ to be eliminated. However, in this work, the maximum number of chained filters is five, since more filters in the chain increase the transient response time to more than about 12ms. A comparison of the maximum notch filter numbers performed is presented in the Section VI(B).

Implementation of the DWPT algorithm in real-time relies on having enough data samples to produce accurate results. A moving data window based on the FIFO scheme is used and the data is held in a buffer. Once the harmonic elements in the power line current are identified by the DWPT-based ANF, their elimination by the MMCC-STATCOM relies on setting the reference current of its current controller. This can

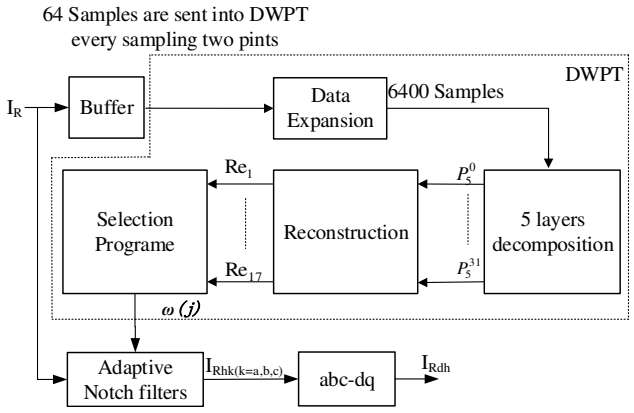


Fig. 8. Schematic of Real-time DWPT harmonic identification.

be achieved by turning the band-stop ANF into a band-pass filter. Fig. 9 shows the implementation of the adaptive band-pass filter for three-phase current. The measured power line three-phase current is processed by the ANF, and the output is then subtracted from the original current. The resultant output becomes the one part of the reference current for the STATCOM controller. The fundamental part is the reactive current.

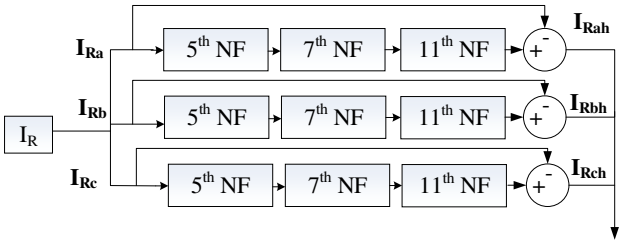


Fig. 9. Implementation of a three-phase band pass filter.

When simultaneous reactive power compensation is required. This can be obtained by either using a PCC voltage control scheme or direct measurement of the reactive load current element. Here the latter method is chosen.

## VI. Simulation Results

To verify the above control scheme for harmonic current cancellation. The power system with the MMCC-STATCOM has been simulated as shown in Fig.1. The system component parameters are listed in table III.

The whole simulation process is designed with four different operation periods as follows:

Period 1: From 0s to 0.05s, the system supplies distorted current to the three-phase thyristor-controlled non-linear load with firing angle 0°. MMCC-STATCOM is disabled, so the converter compensation current IC is zero.

Period 2: From 0.05s to 0.1s, STATCOM is switched on and working to compensate reactive power and harmonic current. The firing angle remains 0°.

Period 3: From 0.1s to 0.2s, STATCOM continuous operating with the load firing angle changes to 30°.

Period 4: From 0.2s to 0.3s, the load firing angle is changed to 45°.

The corresponding current waveforms measured at the PCC are shown in Fig.10. The THD values and ratios of the dominant harmonic elements to fundamental current drawn by the load are listed in Table IV. The fifth harmonic is the most significant, followed by the $7th$ and $11th$. However, when the firing angle is 30°, the $13th$ harmonic increases to above 2% which can not be ignored. Likewise at the firing angle is 45°, the $17th$ harmonic is 4.0% which is higher than 2% and should be eliminated.

TABLE III
Parameters for Simulation

| | |
|---|---|
| Sending end voltage $V_s$ | 110V |
| Inductor L | 2mH |
| Load resistance $R_L$ | 0.1Ω |
| Load inductance $L_L$ | 10mH |
| Capacitor C | 1.12mF |
| Non-linear load resistor | 30Ω |
| Non-linear load capacitor | 1mF |
| Capacitor voltage for each sub-module | 50V |
| Switching frequency | 1KHz |
| Memory Buffer | 64 |
| Sampling frequency | 6400Hz |
| DWPT decomposition layers | 5 |

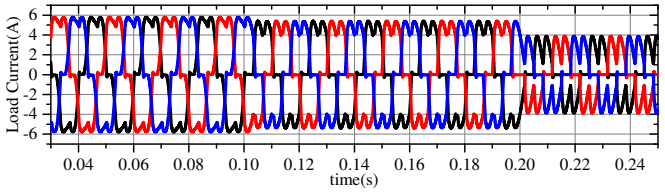


Fig. 10. Load current $I_R$ from non-linear load when firing angle changes from 0° to 30° at 0.1s and from 30° to 45° at 0.2s.

### A. Harmonic detection using DWPT with/without data expansion

Using the data expansion method discussed in Section IV, the identified ratios (%) of the $5th$, $7th$, $11th$, $13th$ and $17th$ harmonic magnitudes to the fundamental current are shown in Fig.11, and that without data expansion are displayed in Fig.12.

Clearly, by applying data expansion method, the transient oscillations of harmonic ratios are lower and they settle down faster than when expansion is not used. Observing the ratios of the $11th$, $13th$ and $17th$ harmonics, shown in Figs.11A(e), (g), (i), identified by the DWPT with data expansion at firing angle 0°, these all have low peak-to-peak values of respectively 0.2%, 0.3% and 0.02%. On the other hand, the harmonic ratios identified by the DWPT without data expansion, for load current with the same the firing angle, are shown in Figs. 12(e), (g), (i), their peak-to-peak values are significantly higher being 1.8%, 1.1% and 0.4% respectively. It is worth noting that, when identified without data expansion, $11th$ and $13th$ harmonics in this period fluctuate and sometimes fall below the required level (2%). This is undesirable since the chained

TABLE IV
THD VALUE AND EACH ODD HARMONIC RATIOS OF $I_R$

| Firing angle | 0° | 30° | 45° |
|---|---|---|---|
| THDs | 20.8% | 27.91% | 32.95% |
| 250Hz($5th$) | 18.1% | 25.65% | 30.49% |
| 350Hz($7th$) | 5.92% | 6.29% | 6.23% |
| 550Hz($11th$) | 2.92% | 6.27% | 8.77% |
| 650Hz($13th$) | 1.41% | 3.34% | 2.86% |
| 850Hz($17th$) | 1.36% | 1.59% | 3.98% |

notch filters in the ANF are set in real-time according to the identify harmonic orders. Frequent variations of the ANF will lead to inaccuracy in harmonic compensation.

When the firing angle is 30°, the peak-to-peak harmonic ratio for the same $11th$, $13th$ and $17th$ harmonics are shown also in Fig.11A (f), (h), (j); with data expansion they are 0.7%, 0.7% and 0.05%.. The results with no data expansion, as shown in Fig.12(f), (h), (j), are significantly higher at 4.0%, 1.0% and 0.6%. Clearly the data expansion method, improves the accuracy and stability of the identified harmonic values.

According to the UK National Grid Code, the nominal frequency is 50Hz, with an allowed interval of 49.5Hz to 50.5Hz under normal operation [40], thus it is necessary to evaluate the performance of the DWPT at the extremes of the grid frequency compared the results with those obtained at 50Hz. Fig.11 shows the DWPT identified harmonic components for these system frequency cases. Note the displayed results for these two frequencies correspond to the period with a load firing angle of 30°and 45°, where the harmonic response performance is considered the worst. It can be seen clearly that the estimated harmonic magnitudes present slightly higher fluctuations than when the frequency is 50Hz, while settling down to their respective steady-states. The patterns of fluctuations repeat every 20ms. This is because the DWPT data window width is set as a half cycle of 50Hz. However, since the ratios of the harmonic amplitudes to the fundamental amplitude frequency are, in general, only about 0.6% higher than at 50Hz, they lead to activating the same group of notch filters as those selected at 50 Hz. For example, as shown in Fig.11B.(a), (b), (c), (d) and (e) when frequency is at 49.5Hz, all oscillation levels are higher than the set criterion for triggering the corresponding notch filter, consequently the same group of notch filters is set and the filtered current THD values measured at the PCC are the same as those when the system frequency is 50Hz. There is only one case which may affect the setting of a notch filter, namely when the frequency is 50.5Hz, the ratio of the $13th$ harmonic (Fig. 11 C.(d)) to the fundamental drops to slightly lower than the 2% limit. This may leads to the corresponding notch filter being cancelled. This, however, has not resulted in a significant negative effect on the performance of the filtered current since the other harmonic elements identified do not fall below the limit (2% or 4%). The current performance is in fact better than that without the data expansion , when the system frequency is 50Hz. Thus it is clear the proposed DWPT+Notch filter scheme will work well with the allowed grid frequency deviations.

In addition to the steady-state fluctuation range of the detected harmonics, the transient performance is also worth noting. In Fig.11, when the firing angle varies at 0.1s and 0.2s using the data expansion method, it takes about 0.01s for the harmonic elements to settle to their steady-state values. However, the transient time intervals are much longer without using data expansion as can be seen in Fig.12. In general, it takes about 0.02s for the harmonic magnitudes to settle to their stable levels.

### *B. Current control results*

Fig.13 shows the waveforms of current $I_S$ measured at the PCC, its d component $I_{Sd}$ , and the STATCOM compensating current $I_C$ , using the ADF combined with DWPT using data expansion. The same current waveforms obtained without data expansion are displayed in Fig.14.

During periods 1 and 2, the load firing angle is 0°, and the identified harmonic orders with ratio above 2% lead to three notch filters being used in the STATCOM control system, namely at the $5th$, $7th$ and $11th$ harmonics. As can be seen in Fig.13(a) the STATCOM is not turned on initially until at 0.05s, so the PCC current waveform is distorted first then becoming sinusoidal when STATCOM is effective. Likewise the d-component of $I_S$, shown in Fig.14(d), is oscillatory first and then becomes a stable DC current with small ripples after 0.05s. These are all due to the output of the STATCOM, whose current $I_C$, as displayed in Fig, 13(g), is zero initially and then active. In contrast, Figs. 14(a), (d) and (g) show the waveform of the current measured at the same points under the same load condition but without data expansion. Clearly in this case, the PCC current contains more ripples than are seen in Fig.13 (a), and the ripple magnitude in $I_{Sd}$ is significantly higher. This is also reflected by comparing the THD values of $I_S$ as shown in table V, the former is 1.91% for the current in Fig.13(a) and the latter is 6.21% for the current shown in Fig.14(a). Clearly the THD value obtained by using the method without data expansion cannot meet the standard set in IEEE-519-2014.

The current waveforms measured during Period 3 when using data expansion are shown in Fig.13 (b), (e) and (h). At 0.1s, the load firing angle is changed from 0° to 30°, correspondingly both the harmonic components and their respective magnitudes in the measured current change. In response, the DWPT in the current control scheme identifies the harmonic elements and subsequently reset the frequencies of the ANF. In this case, the $13th$ order is about 4%, hence the ANF now has 4 notch filters in cascade at of the $5th$, $7th$, $11th$ and $13th$ harmonic frequencies. This process takes about 0.015s, hence the current performance during this transient interval may be affected adversely. As shown in Fig. 13(b), the levels of harmonic contamination in $I_S$ are higher than those during the transient interval from Periods 1 to 2. Even after the transient period, the current waveform performance is slight worsened, since the THD value for PCC current $I_S$ is raised to 2.74% . For the same Period 3, the current waveform obtained when using the DWPT method without data expansion are shown in Fig.14(b), (e) and (h). The $I_S$ fluctuation, during the transient interval after the firing angle changing at 0.1s, is higher and last longer than those shown in Fig.13(b) with use

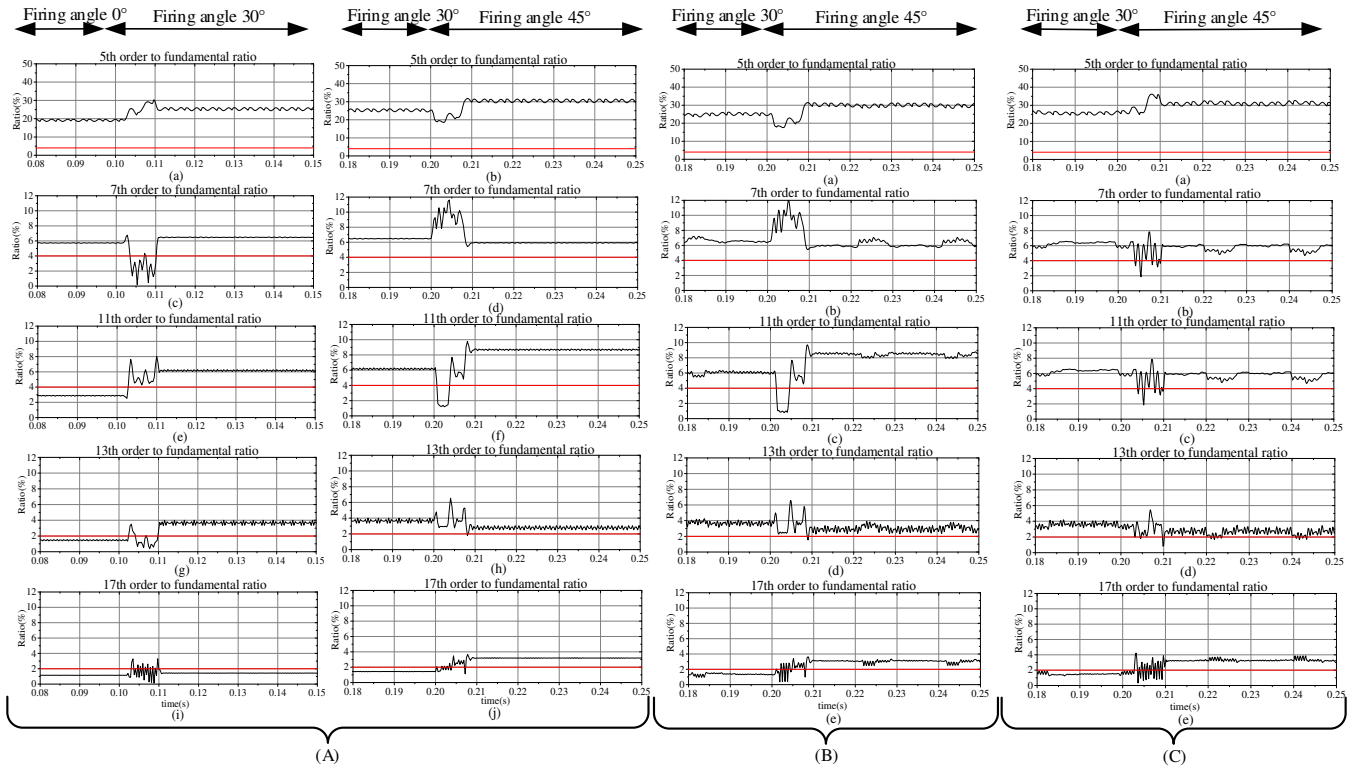


Fig. 11. Variations of the 5th, 7th , 11th, 13th and 17th harmonic to fundamental ratio identified by DWPT with data expansion when power system frequency is 50Hz, 49.5Hz and 50.5Hz. (A)When power system frequency is 50Hz: (a)5th order when firing angle changing from 0° to 30° and (b)from 30° to 45°(c)7th order when firing angle changing from 0° to 30° and (d)from 30° to 45° (e) 11th order when firing angle changing from 0° to 30° and (f)from 30° to 45° (g)13th order when firing angle changing from 0° to 30° and (h) 30° to 45° (i) 17th harmonic when firing angle changing from 0° to 30° and (j)from 30° to 45°.(B)When power system frequency is 49.5Hz and firing angle is from 30° to 45°: (a)5th order when firing angle (b)7th order(c) 11th order(d)13th order (e) 17th harmonic. (C)When power system frequency is 49.5Hz and firing angle is from 30° to 45°: (a)5th order when firing angle (b)7th order(c) 11th order(d)13th order (e) 17th harmonic

of data expansion. According to the THD values of $I_S$ after the transient period dies down, the results from both methods are similar (2.73%), showing that the notch filter frequencies identified by both methods are the same.

The current waveform at periods 3 to 4 when the load firing angle is changed from 30° to 45° are shown in Fig.13(c), (f) and (i) using data expansion, and in Fig.14(c), (f) and (i) without data expansion. In this load condition, the $17th$ order becomes exceeds 2%, hence the number of chained notch filters is increased from 4 to 5 having frequencies at the $5th$, $7th$, $11th$ , $13th$ , and $17th$ orders. Clearly using both methods, the PCC current shows severe distortion during transient interval, though the current waveform in Fig.13 (c) settles more quickly than that shown in Fig.14(c). At steady-state, the current performance obtained with data expansion is better than that without data expansion, since the THD value of $I_S$ for the former is 4.44% (table V), whereas the latter has a THD value as high as 4.87% .

TABLE V
THD VALUES OF PCC CURRENT $I_S$

| Firing angle | 0° | 30° | 45° |
|---|---|---|---|
| With data expansion | 1.91% | 2.74% | 4.44% |
| Without data expansion | 6.21% | 2.73% | 4.87% |

Fig.15 compares waveforms of the PCC current and its d component obtained using four and five notch filters. The response waveform are taken from period 3 to period 4 (in Fig.13), with the firing angle changed from 30° to 45° at 0.2s. In Fig.15 (a) and (c), four notch filters are set for 5th, 7th, 11th and 13th harmonics, and in (b) and (d) an additional notch is added at the 17th. The settling time is initially 8.7ms and is increased by about 2ms in (b) and (d). However, the THD value for the PCC current is reduced from about 5.4% (4 filters) to 4.8% (5 filters). Since the standard THD limit in the input current is set to 5%, the maximum of 5 notch filters is chosen even though its corresponding current response time is slightly longer.

It is notable that the computational burden for the data expansion method is high compared to that of implementing the current control algorithm. To mitigate this burden in the real-time implementation, the DWPT algorithm has been implemented at every other sample instead of every time. As a result, the harmonic estimation result is updated at the frequency of 3200Hz rather than 6400Hz. This gives sufficient time for DWPT algorithm implementation without sacrificing the accuracy. The time delay increase incurred for the notch filter update corresponding to a load change is about 1/3200s and is negligible compared to that for the whole algorithm.

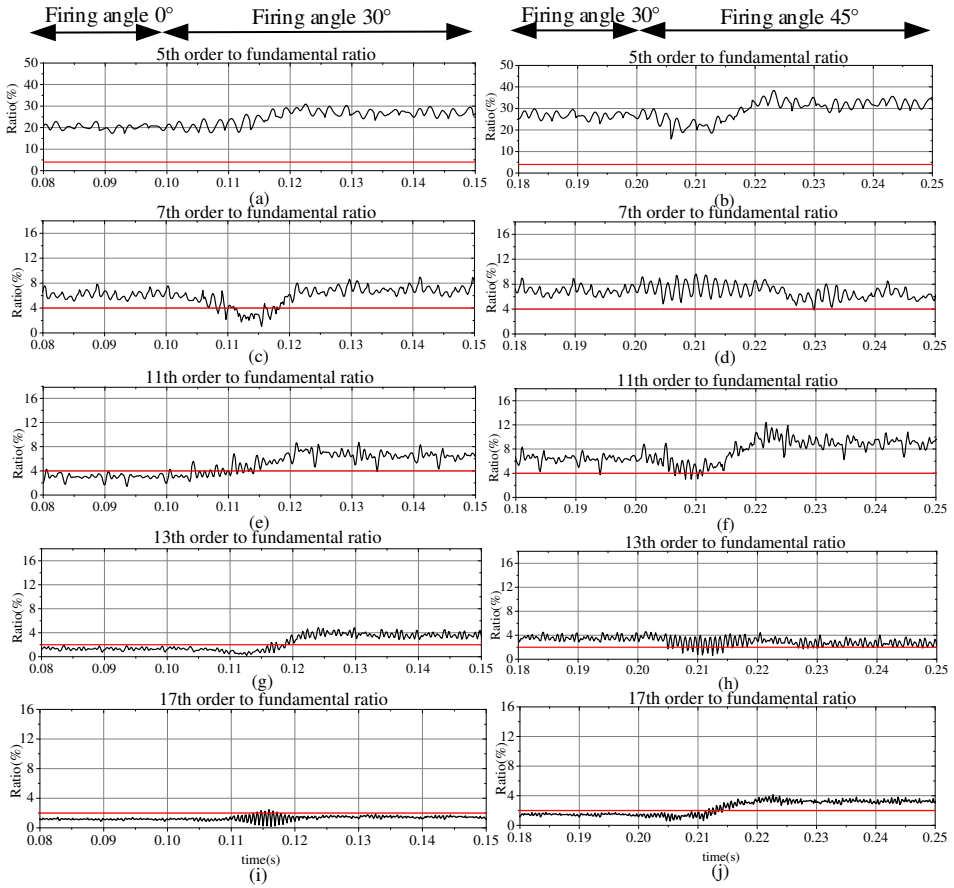


Fig. 12. Variations of the $5th$, $7th$ , $11th$, $13th$ and $17th$ harmonic to fundamental ratio identified by DWPT without data expansion (a) $5th$ order when firing angle changing from 0° to 30° and (b)from 30° to 45°(c) $7th$ order when firing angle changing from 0° to 30° and (d)from 30° to 45°(e) $11th$ order when firing angle changing from 0° to 30° and (f)from 30° to 45° (g)$13th$ order when firing angle changing from 0° to 30° and (h) 30° to 45° (i) $17th$ harmonic when firing angle changing from 0° to 30° and (j)from 30° to 45°.

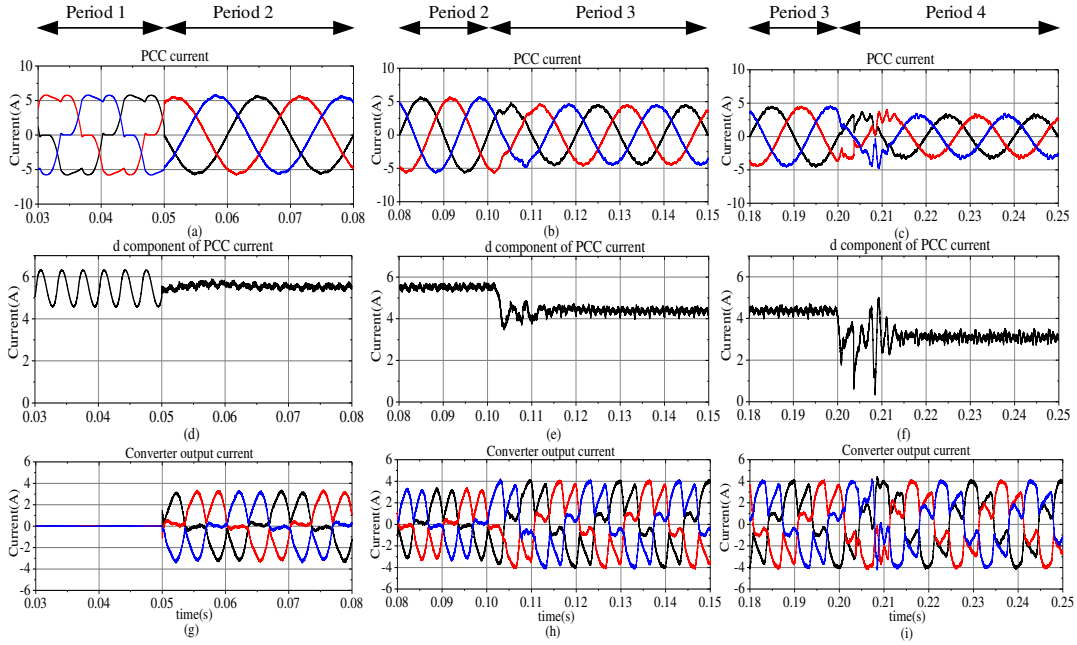


Fig. 13. Variations of current waveforms using method with data expansion: $I_S$ (a)from period 1 to period 2(b)from period 2 to period 3(c)from period 3 to period 4. $I_{Sd}$ (d)from period 1 to period 2(e)from period 2 to period 3(f)from period 3 to period 4. Compensation current $I_C$ (g)from period 1 to period 2(h)from period 2 to period 3(i)from period 3 to period 4

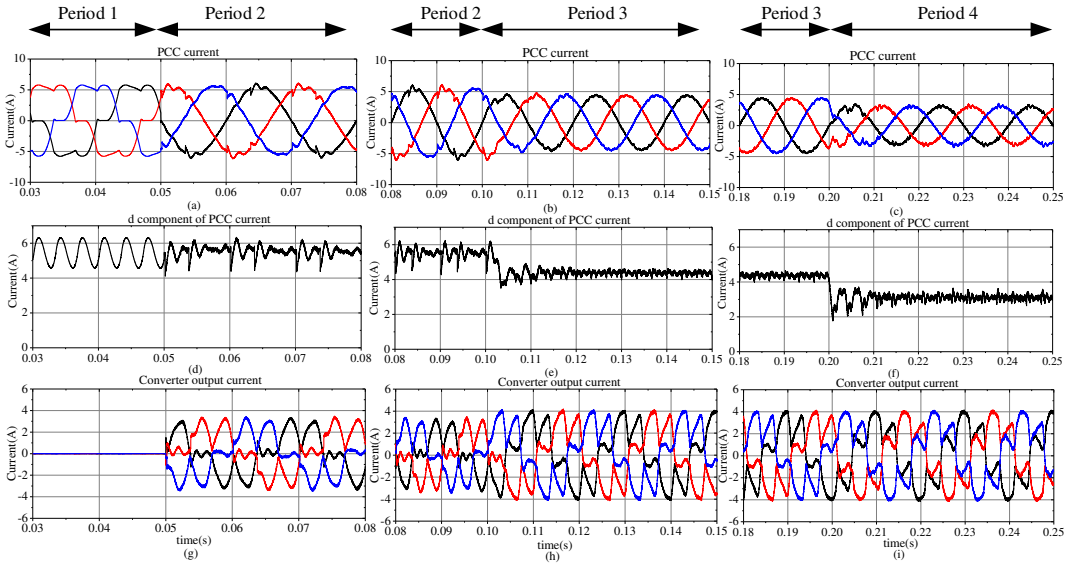


Fig. 14. Variations of current waveforms using method without data expansion: $I_S$ (a)from period 1 to period 2(b)from period 2 to period 3(c)from period 3 to period 4. $I_{Sd}$ (d)from period 1 to period 2(e)from period 2 to period 3(f)from period 3 to period 4. Compensation current $I_C$ (g)from period 1 to period 2(h)from period 2 to period 3(i)from period 3 to period 4

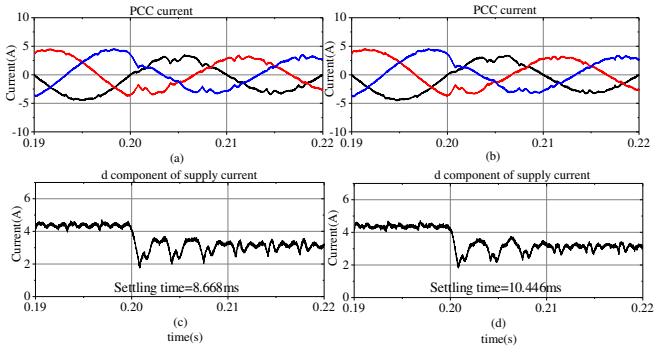


Fig. 15. Variations of current waveforms using method with data expansion: $I_S$ (a)from period 3 to period 4 when maximum number of notch filters is four (b) when the maximum number is 5. $I_Sd$ (c)from period 3 to period 4 when maximum number of notch filters is four (d) when the maximum number is 5.

## VII. Conclusions

The paper proposed a modified DWPT with data expansion method for harmonic extractions of power line current. The results have shown that this method identifies the rms values of the dominant harmonics accurately and responds quickly to the current waveform changes. Importantly the technique was shown to reduce the edge distortion effect compared to the traditional method. The DWPT identifying harmonic elements has been used to update the number and frequencies of a notch filter chain which is embedded in the current control system of an MMCC-STATCOM. The results from harmonic cancellation performed by the STATCOM show that using the DWPT with data expansion, the controller responded faster, with less than 15ms, to the transient changes of the current waveform compared to that without data expansion ( more than 20ms). The accuracy in harmonic cancellation is evaluated according to the THD of the PCC current measured at the steady-states. In all operation conditions, the THD values are lower than obtained using the DWPT without data expansion.

## References

[1] J. M. Carrasco, L. G. Franquelo, J. T. Bialasiewicz, E. Galván, R. C. PortilloGuisado, M. M. Prats, J. I. León, and N. Moreno-Alfonso, "Power-electronic systems for the grid integration of renewable energy sources: A survey," *IEEE Trans. Ind. Electron.*, vol. 53, no. 4, pp. 1002–1016, 2006.

[2] D. Ronanki and S. S. Williamson, "Modular multilevel converters for transportation electrification: Challenges and opportunities," *IEEE Trans. Transp. Electrification*, vol. 4, no. 2, pp. 399–407, 2018.

[3] M. Eremia, C.-C. Liu, and A.-A. Edris, *Advanced solutions in power systems: HVDC, FACTS, and Artificial Intelligence*. John Wiley & Sons, 2016.

[4] L. Wang, C.-S. Lam, and M.-C. Wong, "A hybrid-statcom with wide compensation range and low dc-link voltage," *IEEE Trans. Ind. Electron.*, vol. 63, no. 6, pp. 3333–3343, 2016.

[5] K. Mahapatra, A. Ghosh, and S. Doradla, "Simplified model for control design of statcom using three-level inverter," in *Proceedings of IEEE TENCON'98. IEEE Region 10 International Conf. on Global Connectivity in Energy, Computer, Communication and Control (Cat. No. 98CH36229)*, vol. 2. IEEE, 1998, pp. 536–539.

[6] M. Hagiwara and H. Akagi, "Control and experiment of pulsewidth-modulated modular multilevel converters," *IEEE Trans. Power Electron.*, vol. 24, no. 7, pp. 1737–1746, 2009.

[7] S. Debnath, J. Qin, B. Bahrani, M. Saeedifard, and P. Barbosa, "Operation, control, and applications of the modular multilevel converter: A review," *IEEE Trans. Power Electron.*, vol. 30, no. 1, pp. 37–53, 2014.

[8] H. Akagi, "Classification, terminology, and application of the modular multilevel cascade converter (mmcc)," *IEEE Trans. Power Electron.*, vol. 26, no. 11, pp. 3119–3130, 2011.

[9] N. Hatano and T. Ise, "Control scheme of cascaded h-bridge statcom using zero-sequence voltage and negative-sequence current," *IEEE Trans. Power Del.*, vol. 25, no. 2, pp. 543–550, 2010.

[10] H. Akagi, S. Inoue, and T. Yoshii, "Control and performance of a transformerless cascade pwm statcom with star configuration," *IEEE Trans. Industry Appl.*, vol. 43, no. 4, pp. 1041–1049, 2007.

[11] P.-H. Wu, H.-C. Chen, Y.-T. Chang, and P.-T. Cheng, "Delta-connected cascaded h-bridge converter application in unbalanced load compensation," *IEEE Trans. Industry Appl.*, vol. 53, no. 2, pp. 1254–1262, 2016.

[12] C. Nwobu, I. Efika, O. K. Oghorada, and L. Zhang, "A modular multilevel flying capacitor converter-based statcom for reactive power control in distribution systems," in *2015 17th European Conf. on Power*

*Electronics and Applications (EPE'15 ECCE-Europe)*. IEEE, 2015, pp. 1–9.
[13] H. Akagi, "Generalized theory of the instantaneous reactive power in three-phase circuits," *IEEJ IPEC-Tokyo'83*, vol. 1375, 1983.
[14] S. Bhattacharya and D. Divan, "Synchronous frame based controller implementation for a hybrid series active filter system," in *IAS'95. Conf. Record of the 1995 IEEE Industry Applications Conference Thirtieth IAS Annual Meeting*, vol. 3. IEEE, 1995, pp. 2531–2540.
[15] H. Wen, J. Zhang, W. Yao, and L. Tang, "Fft-based amplitude estimation of power distribution systems signal distorted by harmonics and noise," *IEEE Trans. Industry Infor.*, vol. 14, no. 4, pp. 1447–1455, 2017.
[16] J.-Z. Yang, C.-S. Yu, and C.-W. Liu, "A new method for power signal harmonic analysis," *IEEE Trans. Power Del.*, vol. 20, no. 2, pp. 1235–1239, 2005.
[17] M. Basu and B. Basu, "A wavelet controller for shunt active power filter," in *2006 3rd IET International Conference on Power Electronics, Machines and Drives-PEMD 2006*. IET, 2006, pp. 76–79.
[18] K. K. Gupta, R. Kumar, and H. Manjunath, "Active power filter control algorithm using wavelets," in *2006 International Conf. on Power Electronic, Drives and Energy Systems*. IEEE, 2006, pp. 1–4.
[19] P. Ribeiro, "Wavelets: A new approach to analyze power system distortions," *Proc. EPRI-Power Quality Steering Committee, Baltimore, MD*, 1993.
[20] W. Hou, C. Lu, H. Liu, and C. Lu, "Fault diagnosis based on wavelet package for hydraulic pump," in *2009 8th International Conf. on Reliability, Maintainability and Safety*. IEEE, 2009, pp. 831–835.
[21] R. Yu, "A new shift-invariance of discrete-time systems and its application to discrete wavelet transform analysis," *IEEE Trans. Signal Process.*, vol. 57, no. 7, pp. 2527–2537, 2009.
[22] B. Zhang, H. Chen, G. Feng, and H. Zhang, "Application of wavelet multi-resolution analysis to harmonics detection based on matlab in power system," in *2007 IEEE International Conf. on Automation and Logistics*. IEEE, 2007, pp. 137–143.
[23] S. G. Mallat, "A theory for multiresolution signal decomposition: the wavelet representation," *IEEE Trans. Pattern Anal. Mach. Intell.*, vol. 11, no. 7, pp. 674–693, 1989.
[24] P. Zanchetta, A. Abusorrah, D. Thomas, and M. Sumner, "Power system impedance estimation for improved active filter control, using continuous wavelet transforms." in *2005/2006 IEEE/PES Transmission and Distribution Conf. and Exhibition*. IEEE, 2006, pp. 653–658.
[25] S. H. Jaramillo, G. Heydt, and E. O'Neill-Carrillo, "Power quality indices for aperiodic voltages and currents," *IEEE Trans. Power Del.*, vol. 15, no. 2, pp. 784–790, 2000.
[26] Z.-L. Gaing, "Wavelet-based neural network for power disturbance recognition and classification," *IEEE Trans. Power Del.*, vol. 19, no. 4, pp. 1560–1568, 2004.
[27] H. Erişti and Y. Demir, "A new algorithm for automatic classification of power quality events based on wavelet transform and svm," *Expert systems with applications*, vol. 37, no. 6, pp. 4094–4102, 2010.
[28] N. Kanao, Y. Hayashi, and J. Matsuki, "Analysis of even harmonics generation in an isolated electric power system," *Electrical Engineering in Japan*, vol. 167, no. 2, pp. 56–63, 2009.
[29] J. Barros, M. de Apráiz, R. I. Diego, and E. de Náutica, "Analysis of second order harmonic voltages in power systems," in *International Conference on Renewable Energy and Power Quality*, vol. 2007, 2007, pp. 1–5.
[30] P. Chittora, A. Singh, and M. Singh, "Harmonic current extraction and compensation in three phase three wire system using notch filter," in *2015 IEEE Recent Advances in Intelligent Computational Systems (RAICS)*. IEEE, 2015, pp. 422–427.
[31] D. Yazdani, A. Bakhshai, G. Joos, and M. Mojiri, "An adaptive notch filtering approach for harmonic and reactive current extraction in active power filters," in *2008 34th Annual Conf. of IEEE Industrial Electronics*. IEEE, 2008, pp. 535–538.
[32] R. LANGELLA, A. TESTA, and E. Alii, *IEEE recommended practice and requirements for harmonic control in electric power systems*. IEEE, 2014.
[33] V. K. Tiwari, A. C. Umarikar, and T. Jain, "Fast amplitude estimation of harmonics using undecimated wavelet packet transform and its hardware implementation," *IEEE Trans. Instrum. Meas.*, vol. 67, no. 1, pp. 65–77, 2017.
[34] Z. Guojiang, S. Mingming, Z. Chenyu, S. Haoyuan, and S. Changjia, "Harmonic impedance detection based on capacitor switching and wavelet packet analysis," in *2019 IEEE 9th Annual International Conf. on CYBER Technology in Automation, Control, and Intelligent Systems (CYBER)*. IEEE, 2019, pp. 497–502.
[35] A. Srivastava, A. Siddharth, A. K. Singh, and A. K. Singh, "Some observations on selection of most suitable mother wavelet for measurement of power system harmonics using cwt," in *TENCON 2009-2009 IEEE Region 10 Conf.* IEEE, 2009, pp. 1–6.
[36] A. Megahed, A. M. Moussa, H. Elrefaie, and Y. Marghany, "Selection of a suitable mother wavelet for analyzing power system fault transients," in *2008 IEEE Power and Energy Society General Meeting-Conversion and Delivery of Electrical Energy in the 21st Century*. IEEE, 2008, pp. 1–7.
[37] D. K. Alves, F. B. Costa, R. L. de Araujo Ribeiro, C. M. de Sousa Neto, and T. d. O. A. Rocha, "Real-time power measurement using the maximal overlap discrete wavelet-packet transform," *IEEE Trans. Ind. Electron.*, vol. 64, no. 4, pp. 3177–3187, 2016.
[38] M. A. Coffey, "Boundary-compensated wavelet bases," in *1997 IEEE International Conf. on Acoustics, Speech, and Signal Processing*, vol. 3. IEEE, 1997, pp. 2129–2132.
[39] P. A. Regalia, S. K. Mitra, and P. Vaidyanathan, "The digital all-pass filter: A versatile signal processing building block," *Proc IEEE Inst Electr Electron Eng*, vol. 76, no. 1, pp. 19–37, 1988.
[40] N. Jenkins and J. Ekanayake, *Renewable energy engineering*. Cambridge University Press, 2017.

**Xuejiao Pan** was born in Wuxi, Jiangsu, China in 1994 and received B.Eng. degree in Electrical Engineering from Nantong University, Nantong, Jiangsu, China in 2016. He received M.Sc. degrees in Electronic/Electrical Engineering from University of Leeds, United Kingdom in 2018.

He is currently studying Phd degree at the Electronic/Electrical Engineering from University of Leeds, United Kingdom. His research interests include modulation and control of power converters, multilevel converters, modular multilevel converters, FACTs devices, Harmonic cancellation methods.

**Li Zhang** (M'03-SM'10) received the PhD degree and was a research fellow in Oxford University, UK. She was then a lecturer at the University of Bradford and is currently a senior lecturer in the School of Electronic and Electrical Engineering at the University of Leeds, UK. Dr Li Zhang is an adjunt professor in Chongqing University, China from 2006 till now and Joint Grant holder of China State Natural Science Foundation Fund (60712, 2014 01-2017 12) entitled: Analysis and research on the hot spot effect and it's control method of photovolaic system. She is an associate editor for IEEE, Transaction on Power Electronics and has also been the associate editor of IET proceedings on Power Electronics between 2014 to 2017. She has authored and co-authored three books on power converter circuits and wind power electricity generation. She has authored and co-authored more than 130 technical papers in the fields of power electronics, renewable power generation system and wind generator control.

**Han Huang** (S'17-M'19) received the Ph.D. degree in Electronic and Electrical Engineering from University of Leeds, Leeds, U.K., in 2019.

He worked as a Postdoctoral Researcher with the Energy Safety Research Institute, Swansea University, Swansea, U.K. In 2021, he joined the HVDC Centre of Excellence, GE's Grid Solutions, Stafford, U.K., as a Lead Electrical Engineer.

His research interests include modular multilevel converter control, HVDC system design, FACTs and integration of renewable energies into the power grid.